# 3D digital image correlation analysis of medium velocity soft impacts on laminated composite

Olivier Dorival, Pablo Navarro, Steven Marguet, Jean-François Ferrero

# 3D digital image correlation analysis of medium velocity soft impacts on laminated composite

O. Dorival[a, b], P. Navarro[a], S. Marguet[a], J.-F. Ferrero[a]

[a] *Université de Toulouse, Institut Clément Ader, UMR CNRS 5312, INSA/ISAE/Mines Albi/UPS, 3 Rue Caroline Aigle, 31400, Toulouse, France*

[b] *Icam School of Engineering, Toulouse campus, 75 avenue de Grande Bretagne, 31300, Toulouse, France*

**Abstract**

In aerospace acamedic and industrial world, soft impacts are commonly used to replace bird strike tests for the validation of materials and structures as well as the calibration of numerical models. However in general, the analysis reported show only a few part of the experimental information available. In this paper, three laminate composites made of epoxy resin reinforced by glass or carbon fibres are tested under gelatin impact at several velocities up to complete failure. A detailed analysis based on 3D Digital Image Correlation (3D DIC) and visual inspection of the three laminates is provided for a total of 21 tests with impact velocities in the range 60-112 m/s. DIC extraction provides accurate quantitative displacement fields of the rear face in both time and space. Moreover, specific failure scenarios are identified for each laminate. The results obtained provide a suitable database for the development of numerical models. In addition, all experimental data from DIC extractions are opened to the readers on the *Recherche Data Gouv* website for comparisons with their own tests or numerical models.

*Keywords:* bird strike, gelatin, laminated composites, digital image

correlation, damage of composites, gas gun test, experimental transient dynamics, carbon/epoxy, glass/epoxy

## 1. Introduction

As a major threat in the aeronautical area, impact loading has received close attention over the past decades. Not only for aircrafts but also for helicopters, impact events such as bird strikes, impact with hailstones, metal debris, tyre debris, drone, etc. are likely to damage vital parts of aircrafts and helicopters such as fuel tanks [1], windshields [2, 3, 4], wings [5, 6, 7, 8], engine blades [9, 10], rotor blades, rotor parts, or flying instrument such as Pitot tube. At the design stage, this requires to evaluate the resistance of structures to such severe loadings whenever the material is modified. In particular, increasing use of laminate or sandwich composites in structural parts [11, 12, 13], favored by their high stiffness to weight ratio, is still given a special focus due to the competition between several failure mechanisms [14, 15] and large number of design parameters.

This study focuses on bird strikes for which number of catastrophic events have been reported in the past decades, as reviewed for instance in [16, 17]. Early experiments were performed by Barber [18], in which small birds (60 gr. to 125 gr.) were shot perpendicularly to a rigid target. The pressure time histories recorded were composed of a low frequency signal starting with a peak pressure followed by a steady state flow, plus a high frequency signal attributed to bird heterogeneity. In [19] the study was completed with a limited number of impacts with larger birds (0.9 to 3.6 kg) but no steady state phase was found in this case. Effects of oblique impact and target compliance

were also briefly investigated. A hydrodynamic model was developed by Wilbeck [20] that allows to calculate the peak pressure (Hugoniot pressure), the steady-state pressure (stagnation pressure) and the impact duration. The model was compared with real birds and substitute bird material and some differences were reported, in particular for real birds due to large scatter. It is worth noting that despite the inevitable simplifications of Wilbeck's 1D model (already mentioned by Wilbeck himself), the equations still serve as a reference for quick but yet reasonably precise evaluation of the Hugoniot and stagnation pressure onto the target. However, this theory was developed for rigid targets only. It cannot capture the time-space repartition of the pressure, nor effects such as of waves reflection, target compliance, target shape, projectile shape, etc. For instance, large differences in the shock pressure between Willbeck's theory and experiments were reported in [21].

Since then, several numerical methods to solve the dynamic fluid-structure interaction problem have emerged with the ambition to provide designers with a much more detailed model. A precise representation of the physics involved could tackle the problem up to the prediction of damage in the structure. As reviewed in [22], a huge number of papers have been devoted to the development of numerical methods. The most promising strategies are based on Smooth Particle Hydrodynamics (SPH) methods or Arbitrary Eulerian Lagrangian (ALE) approaches. The validation of these numerical approaches is usually made by comparisons with Wilbeck's theory (despite simplified) or confronted to experimental results that generally use substitute birds like gelatin projectiles for instance. The question of the validity of replacing real birds by substitute materials is still discussed. In [23] for instance, very few

impacts with 1.8 kg birds showed differences between gelatin and real birds. Consistent with this, Lavoie [24] measured a drop in the velocity of the projectile end during the past half of the impact while Wilbeck's theory assumes constant velocity during the flow to calculate the impact time. Nevertheless, in the academic world as well as in aircraft industry, gelatin impact tests are commonly used for testing structures under soft impact sollicitation.

Such soft impact experiments are challenging to perform, and most of the time, a very limited experimental information is extracted from the tests, which limits the validation of numerical models. This is also questionable because one ambition of numerical models is to help the design process with a very detailed local space-time information, what would need to validate the models with this scale of representation. In [25], the failure modes caused by bird strike to metallic or composite plates and half-rings were the only data studied. Most of the time, the time history of deflections or strains taken at the center or at a few points in the sample were compared to the numerical results [2, 26, 27, 28, 29]. In [30], Fiber Bragg Grating (FBG) sensors were used to record the strain on the back face of a small representative segment of front fairing of an helicopter. The structure tested to soft impact was a curved rectangular sandwich structure made of a 20 mm thick closed-cell polymeric foam core with relative high stiffness and strength and low density, and two 2.88 mm thick quasi-isotropic carbon fibre reinforced plastic (CFRP). In [31], impact absorption of two reinforced composite sandwich panels were tested against bird strike with the main information - apart the impact velocity - being the internal damage inspection by pulse thermography and X-ray CT. The sandwiches consisted in two facesheets made of 1 mm thick woven

carbon fibre prepreg, and a low density polyurethane foam core reinforced with either a corrugated carbon composite sheet, or orthotropic carbon fibre twill prepreg tubes.

The resulting force and the momentum imparted onto the structure can also be compared [32]. In particular, one question in the field is the amount of momentum transfered to the structure in the case of normal or oblique impacts. In [33], the momentum transfer on three rigid targets (a plate, a wedge and a splitter) was studied experimentally and numerically in order to quantify the forces originating from the change of momentum and splitting of the bird. A precise measurement of the pressure field is still beyond capabilities. Direct point pressure measurements with carbon gages have been reported to lead to unacceptable values in [24]. It could be due to impedance effects between the projectile and the target as explained in [34], who proposed to use a simple force sensor to derive the average pressure (but not the pressure field) during the shock. It was shown that it is necessary to account for the acoustic impedance of the sensor in order to achieve reliable values of the dynamic pressure.

The radial expansion of the projectile, that can be compared with Wilbeck's model or numerical models, is also easily extractable from impact tests up to a given precision. This is a very interesting information since it strongly depends on the material behavior in large deformation and at high strain rate. While [30] found good agreements with SPH simulations, results of [35] indicate that "models predict less accurately the radial expansion, especially at lower impact velocities", pointing out the need of improvement in the material model for the substitute bird.

In the recent years, the development of digital image correlation (DIC) has provided a very efficient tool for the analysis of specimen deflection as it gives a field information over the visible area of the sample along the time evolution. Although it was already mentioned in [36] as one of the promising techniques to study strain rate effects in highly dynamic problems, to the authors knowledge it has not been widely used for birds strike tests. The main technical difficulty is to record with high frequency devices, and in particular to synchronize the different cameras with each other. The scope of this paper is to present this experimental technique as the best candidate to validate numerical models since the experimental information is very rich. Use of DIC for various type of impulsive loadings has been briefly reviewed in [37]. To study severe dynamic loadings, high-speed digital image correlation has been used, for instance for low velocity impacts [38], air blast [39, 40], dynamic Brazilian test [37]. High-speed stereo-digital image correlation is capable to provide the time history of 3D displacement field of the sample face and, by differenciation, the in-plane strains. For bird impacts, it should be applied on the back face of the sample because the face impacted is blurred by the gelatin flowing on the target. However, despite the very rich information available from DIC, the comparison between experiments and numerical models have so far been limited to a very partial information. In [41], only the central deflection (both dynamic and residual) was extracted from DIC and, together with forces on the test rig, compared with SPH simulations with the idea to validate a bird substitute material model for the helicopter flight domain. In [3, 4], 3D DIC was used on a small part of a laminated windshield and a similar trend was found between SPH simulations and experimental results.

Quantitative comparisons were mainly given at a few points: the central out-of-plane displacement and center or off-center major principal stain. Note that the deflection profile along an horizontal line was also plotted, and can be considered as a premice of a field validation of the simulations. A similar approach was used in [42].

The objective of this paper is to analyze gelatin impact tests performed on three laminated composites based on 3D DIC data. Tests with various impact velocities were performed on each type of material up to failure. The materials tested and the experimental set up are described in Section 2. One aim of this paper is also to provide some DIC data available as an open material for potential validation of numerical methods. To this aim, results of experimental natural modes and frequencies obtained by free-free tap tests are also given in Section 2 to allow stiffness and mass calibration. The results of impacts tests are given in Section 3 based on the analysis of DIC data, strain gages and visual inspection. All experimental data from DIC analysis are open to the readers on the *Recherche Data Gouv* website at the following URL [43]: https://doi.org/10.57745/UA1CRZ. Conclusions are then given in Section 4.

## 2. Materials and experimental set-up

### *2.1. Specimen description*

Three laminated composites (10 specimens each) were provided by Multiplast company in the framework of the projet named SUCCESS. The stacking sequences are detailed in Tab. 1. Laminate 1 is composed of 16 plies of plain weave fabrics prepreg made of epoxy resin reinforced by glass fibres. The

nominal areal mass is 600g/m$^2$ for the 14 inner plies, and 300g/m$^2$ for the upper and lower ones. Laminate 2 is composed of 20 prepreg plies of epoxy resin reinforced with equivalent T700 unidirectional (UD) with a nominal areal mass of 300g/m$^2$ for each ply. Laminate 3 is composed of 20 prepreg plies of UD or plain weave fabrics made of epoxy resin reinforced with equivalent T700 carbon fibres with a nominal areal mass of 300g/m$^2$. Stackings were compressed at 0.8 bar minimum each 1 or 2 plies during 10 minutes. The curing conditions for laminate 1 use a temperature ramp rate of 0.3°C/min, followed by a first plateau at 80°C during 1 hour and a second plateau at 92.5°C during 6 hours. For laminates 2 and 3, the ramp rate is 0.5°C/min, followed by a first plateau at 80°C during 3 hours and a second plateau at 100°C during 5 hours. After curing, composite plates were cut in 400mm × 400mm samples. The masses and thicknesses measured are given in Tab. 2.

| Designation | Stacking |
|---|---|
| Laminate 1 | glass-epoxy plain weave fabrics<br>$[(0-90)^f/(0-90)^f_{14}/(0-90)^f]$ |
| Laminate 2 | carbon-epoxy unidirectional<br>$[45/-45/0/90/45/-45/0/90/45/0/90/-45/90/0/-45/45/90/0/-45/45]$ |
| Laminate 3 | carbon-epoxy unidirectional & plain weave fabrics<br>$[(\pm 45)^f/(0)^{UD}_3/(\pm 45)^f/(0)^{UD}_3/(90)^{UD}_2]_{\text{sym}}$ |

Table 1: Specimen tested. $^{UD}$ and $^f$ denotes a unidirectional ply and fabric ply respectively.

In order to allow models calibration, the basic modal properties of the samples have been tested by tap test in free-free boundary conditions. The

| Designation | Areal mass [kg/m$^2$] (measured) | Thickness [mm] (nominal) | (measured) |
|---|---|---|---|
| Laminate 1 | 13.075 ±0.1875 | 8.5 | 7.29 ±0.83 |
| Laminate 2 | 9.231 ±0.1875 | 5.5 | 6.16 ±0.23 |
| Laminate 3 | 9.294 ±0.1875 | 5.5 | 6.43 ±0.13 |

Table 2: Sample properties measured.

sample plate was hanging on sandows to mimic free-free boundary conditions. The experimental mesh was a $5 \times 5$ grid with 90mm between each point. The accelerometer was fixed at corner (1, 1) and the hammer was moved at each point of the grid. The tap tests were performed in the range [0-5000 Hz] with a frequency resolution of 0.15 Hz (32768 lines). 10 measures per point and Hanning windowing were used. The force and acceleration signals were then treated by dBFA Suite software to obtain the Frequency Response Functions (H1-estimator) and extract the modal properties with Star7 modal analysis software. The natural frequencies, mode shapes and modal dampings are given in Fig. 1, 2 and 3 for laminates 1, 2, 3 respectively. To help numerical model construction, ply properties obtained in the framework of the project SUCCESS [44] by calibration between the experimental natural frequencies and the numerical ones are given in Tab. 3.

### *2.2. Experimental set-up*

The soft impact tests were performed on the STIMPACT platform at Institut Clément Ader, Toulouse, France. This apparatus is classically used for reproducing impact events such as bird strikes or debris or hail impacts. The gas gun impact set-up is shown in Fig. 4.

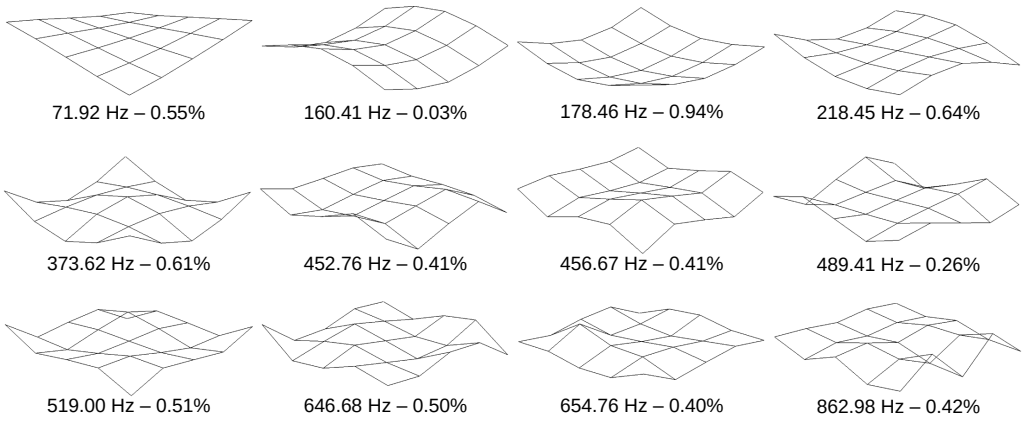


Figure 1: Experimental modal analysis on laminate 1: natural frequencies, modal shapes and modal dampings.

The gas gun used is composed of a pressurized air tank closed by a PET membrane. At a given pressure, the membrane breaks and a pressure wave is released in a 120mm diameter tube. A 750g gelatine projectile, stabilized in a sabot made of foam, is accelerated during its course in the tube. At the exit

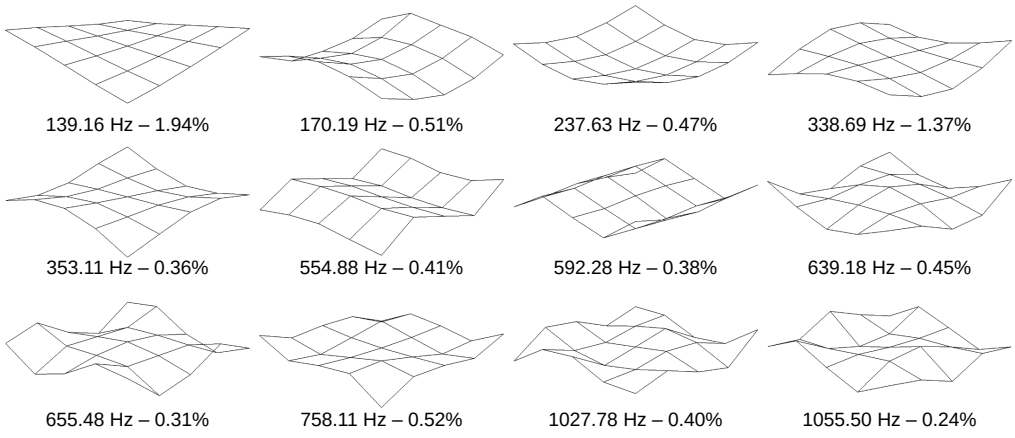


Figure 2: Experimental modal analysis on laminate 2: natural frequencies, modal shapes and modal dampings.

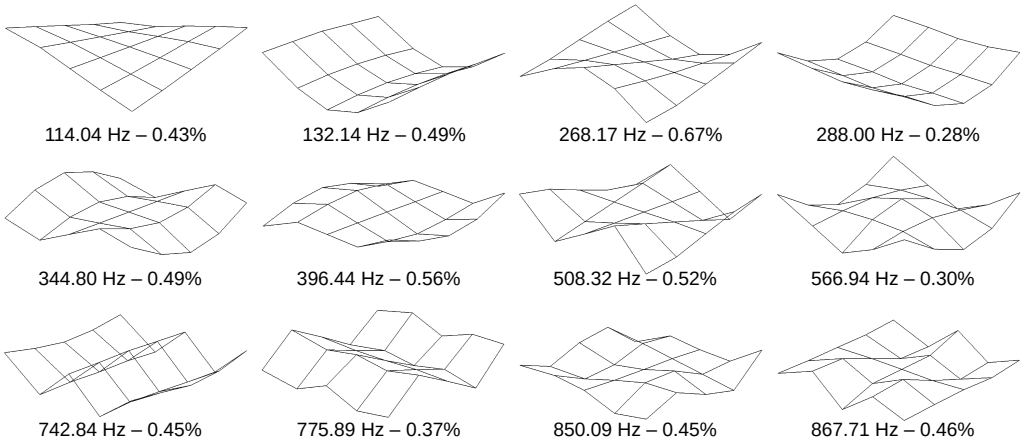


Figure 3: Experimental modal analysis on laminate 3: natural frequencies, modal shapes and modal dampings.

| Glass-epoxy plain weave fabrics | | |
|---|---|---|
| Longitudinal elastic modulus $[GPa]$ | $E_{11}$ | 34.14 |
| Transverse elastic modulus $[GPa]$ | $E_{22}$ | 10.04 |
| In-plane shear modulus $[GPa]$ | $G_{12}$ | 3.032 |
| Poisson's ratio | $\nu_{12}$ | 0.297 |
| Carbon-epoxy UD | | |
| Longitudinal elastic modulus $[GPa]$ | $E_{11}$ | 137.6 |
| Transverse elastic modulus $[GPa]$ | $E_{22}$ | 8.98 |
| In-plane shear modulus $[GPa]$ | $G_{12}$ | 3.66 |
| Poisson's ratio | $\nu_{12}$ | 0.281 |

Table 3: Ply properties used in [44].

of the tube, a deflector allows to deviate the foam sabot from the projectile, in order to ensure that only the gelatine impacts the composite structure. For a given projectile mass and pressure released, the length of acceleration

in the tube leads to a given impact velocity when the projectile reaches the sample plate. The impact velocity has been adapted in order to provoque gradual damage. The range of velovities (resp. trigger pressure) was 87-112 m/s (resp. 1.64-2.37 bar) for laminate 1, 64-105 m/s (resp. 0.93-2.19 bar) for laminate 2, 60-90 m/s (resp. 0.82-1.71 bar) for laminate 3. Details of velocities and pressure measured are given in Tab. 4-6.

The projectile shape consists of a 100 mm diameter cylinder terminated by a spherical edge (for the impact side) and a flat edge (for the back side). The head of the projectile was painted in order to help the localization of the projectile on the camera pictures. Following [24], the projectile was composed of 10% porcine gelatin mixed in hot water and cooled at least 8 hours at fridge temperature before testing. The projectile density used in [44] was 950 kg/m$^3$. Since gelatin properties are likely to vary due to drying, impacts tests were performed maximum 24h after moulding.

The composite sample plate leaned on a 50mm thick aluminum support plate. Clamped conditions, which are commonly used because of technical simplicity, have been reported to create shear stresses near the clamping, which could initiate damage in the structure [45, 46, 47]. Also, clamped boundary conditions are less reliable for numerical models as the deformation of the support frame is not accounted for. Since in real conditions, strains due to bending deflection and not the pressure wave itself was suspected to be the main reason for creating damage, simply supported boundary conditions appeared more suitable to characterize damage for a given impact condition. In order to favour it, the aluminum support plate was machined with a 350mm diameter hole in its center and then chamfered to obtain a 360mm

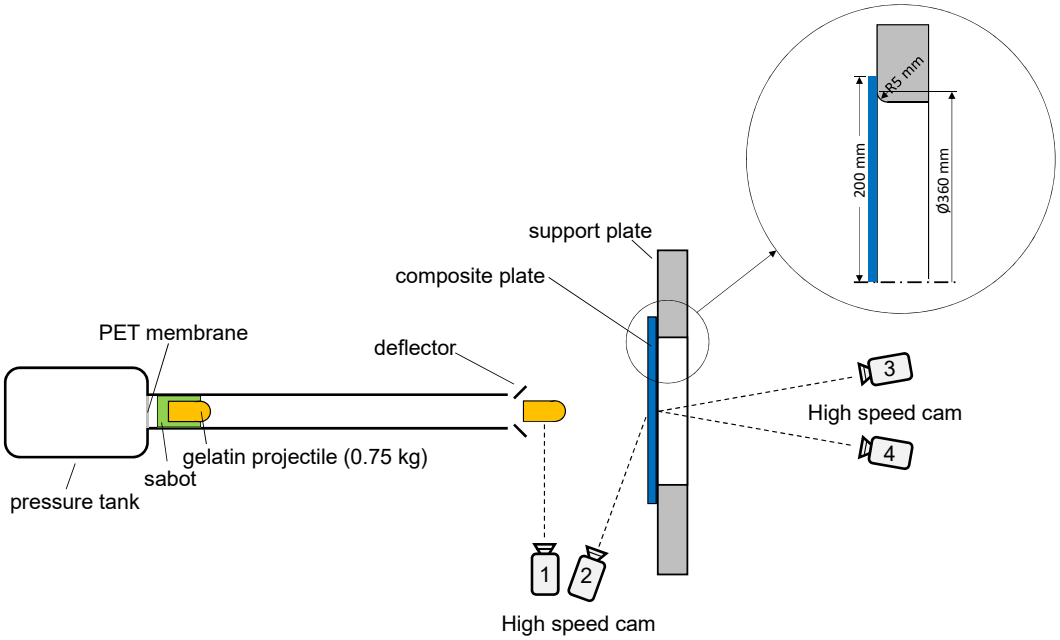


Figure 4: Gas gun setup used for gelatin impact tests with 3D DIC devices (STIMPACT platform).

cylindrical simply supported boundary condition during the impact. The complete set-up is shown in Fig. 5. Small parts and shelf brackets that fixed the support plate allowed to adjust the position in order for the composite plate center to coincide with the impact center.

The instrumentation mainly consisted of four fast cameras (SA5 model 1300K-M3) : two ahead of the plate, and two behind the support plate, see Fig. 4:

- camera 1 recorded the projectile at the exit of the tube. It was used to measure the initial speed of the projectile and to check the deflection of the sabot;

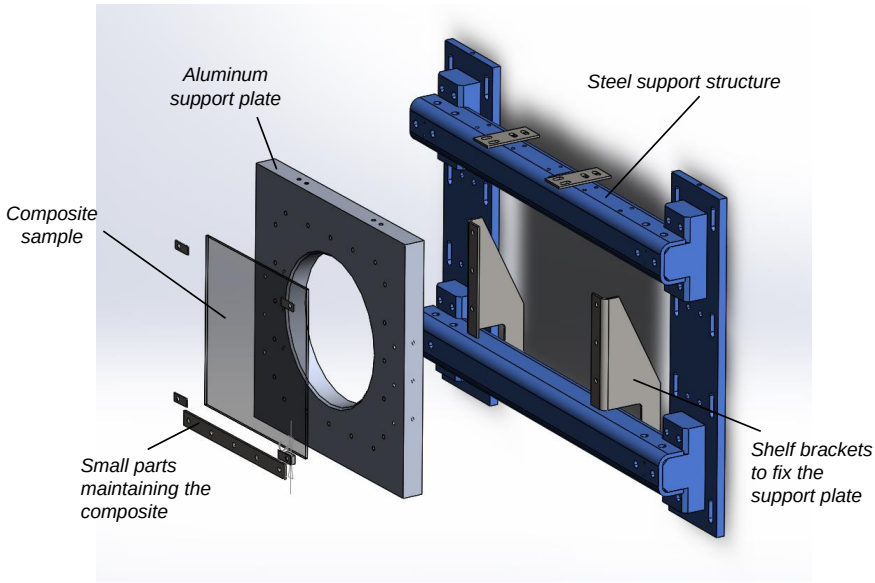


Figure 5: Composite specimen with simply supported set-up.

- camera 2 recorded the impact of the projectile on the sample. It was used to check that the impact is located at the center of the plate;

- cameras 3 and 4 recorded the deflection of the composite plate on the back face. The aim was to use 3D DIC to obtain the displacement field of the plate.

In order to perform 3D digital image correlation analysis, a speckle was painted on the back face of the sample plate as shown in Fig. 6 (left). The support plate was also speckled in order to get a fixed reference. The speckle was composed of random dark spot adapted in order to improve the resolution of DIC analysis with respect to the image size. The order of magnitude was 3-5 pixels per dark spot. 704x512 pixels$^2$ was the maximum image size available on the cameras at the 20000 img/sec sampling frequency

considered, with shutter speed equal to 1/34000 sec. The scene was lighted by six light spots. The DIC analysis was performed with VIC3D software with a subset size of 23x23 pixels$^2$, see Fig. 6 (right). In particular, it allowed to check that, contrary to [41], the frame remained fixed during the impact event.

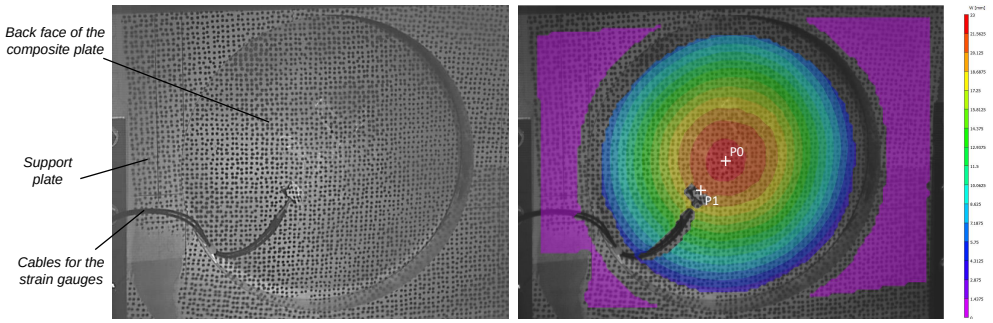


Figure 6: left: support plate and specimen back face speckled; right: 3D DIC analysis performed with VIC3D software.

Eventually, 350Ω strain gauges were glued on the back face in order to check that 3D DIC analysis was suitable for the computation of strains on the back face. Strain gauges were oriented in the same direction as the back ply fibres: 0° for laminate 1, and 45° orientation for laminates 2 and 3. When used, two strain gauges were glued: one at the center of the plate (denoted by P0), the other at 75mm from the center (denoted by P1), on a line in the direction of the back ply orientation. A drawback is that the gauge cables may obstruct the DIC extraction, see Fig. 6 (right). Eventually, the gauges may also be peeled due to the propagation and reflexion of impact stress waves. An example of strain signals for an impact performed at 68 m/s on laminate 3 is shown in Fig. 7. Strains calculated by DIC extraction agrees very well with the signals measured by the strain gauges, despite that high

frequencies were filtered by DIC subset averaging process. After several trial tests, 3D DIC analysis was found to provide reliable data with respect to the strain gauges. For these reasons, strain gauges were abandoned for the next tests and 3D DIC was considered the main source of experimental data.

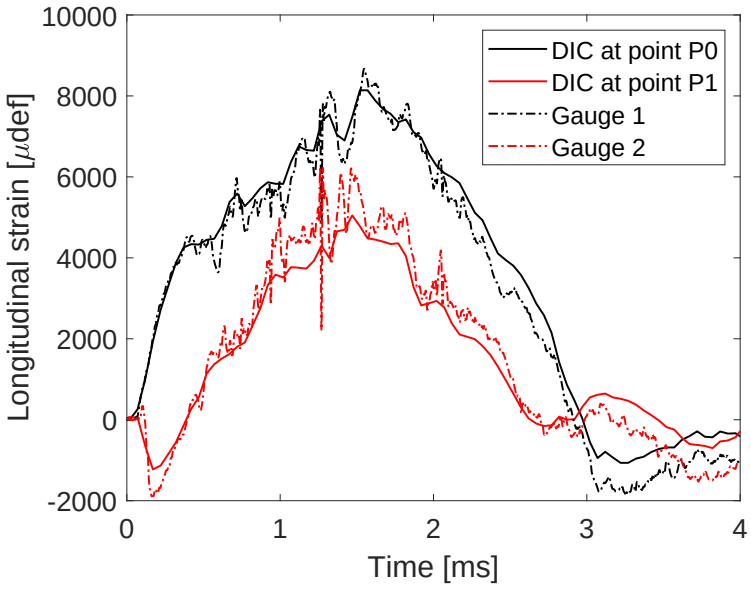


Figure 7: Validation of 3D DIC by strain gauges results. Laminate 3 impacted at 68 m/s. Points P0 and P1 are shown in Fig. 6.

## 3. Results and discussion

### *3.1. Example: laminate 1 impacted at 92 m/s*

Fig. 8 provides an example of impact recorded by the impact camera on laminate 1 at 92 m/s . Immediatly after the impact, the gelatin projectile flows radially from the plate center. At time $t \simeq 1700$ $\mu$s the whole length

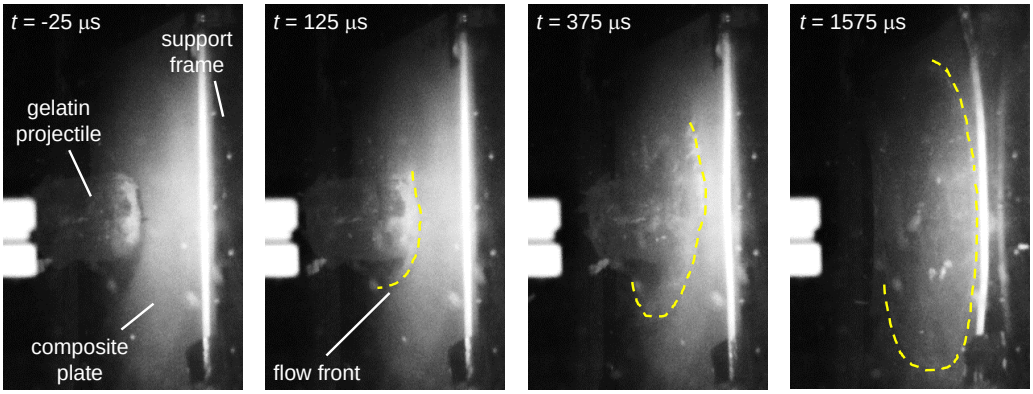


Figure 8: Impact recorded for laminate 1 impacted at 92 m/s.

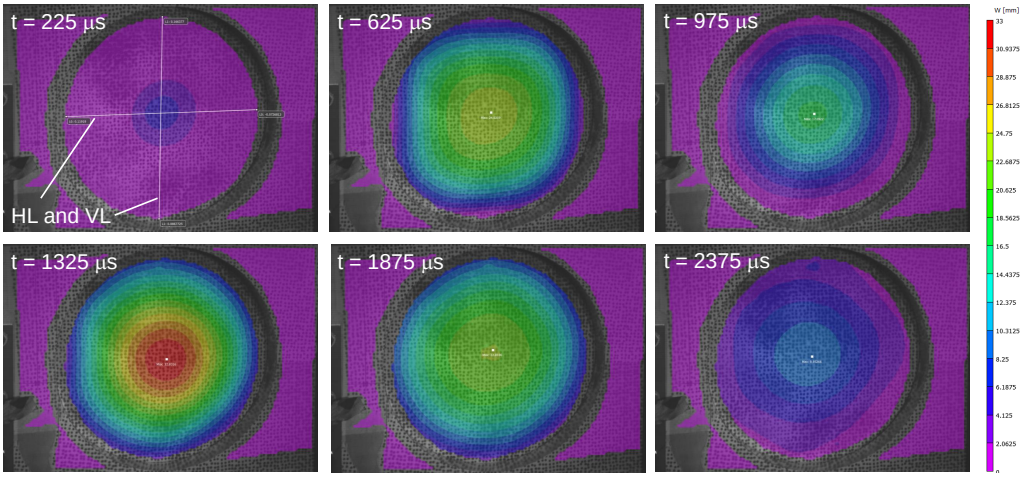


Figure 9: DIC extraction at various time steps for laminate 1 impacted at 92 m/s.

has flowed and the projectile has a "pancake" shape. As discussed later, this time is slightly longer than the time obtained theoretically by dividing the projectile length by the impact velocity. During most of the experiments, the projectile regained its initial shape after impact due to elastic return, or was eventually found destroyed into a few gelatin parts for the highest impact velocities.

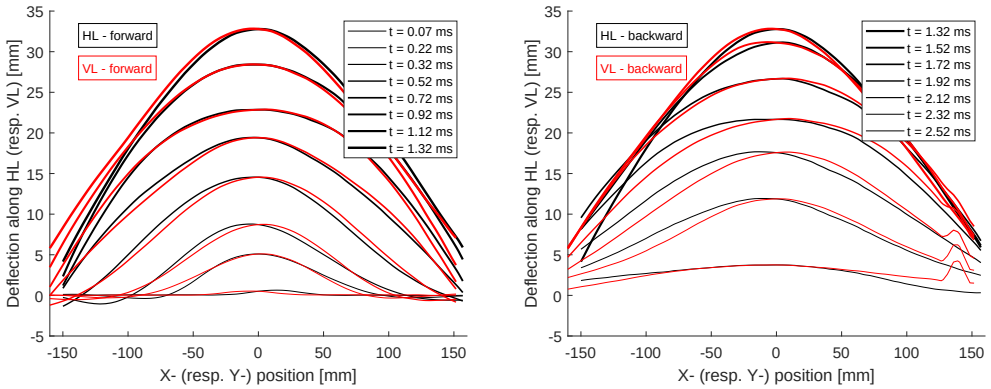


Figure 10: Deflection along horizontal line HL (black) and vertical line VL (red) at various time during the forward (left) and backward (right) motion for laminate 1 impacted at 92 m/s.

The corresponding 3D DIC extraction shown in Fig. 9 illustrates the progressive deflection of the sample plate. In the DIC extraction, time $t = 0$ was defined as the last picture for which the out-of-plane deflection remained below a treshhold of 0.1 mm, roughly corresponding to the noise before impact. As the gelatin reaches the structure, only the center of the plate deflects during the first microseconds. The deflection then increases and quickly propagates towards the edges. Maximum deflection takes place at around 1300 $\mu$s. After that, elasticity causes the plate to deform backwards to zero, then back and forth into negative and positive directions during number of oscillations. The duration of 1300 $\mu$s to reach the maximum deflection roughly corresponds to a quarter of the natural period of the first bending mode with the simply supported conditions imposed by the set-up.

Fig. 10 shows the out-of-plane displacement at various time steps along the central horizontal line (HL) and vertical line (VL) during the forward and

backward motion. Lines HL and VL are depicted in Fig. 9. For laminate 1, the stiffnesses in the 90° and 0° directions are equal, what can be checked experimentally by comparing the shapes between the deflections along HL and VL in Fig. 10. The strange deflection measured along VL during the backward motion at $Y \simeq 140$mm is due to a debris crossing the pictures and blurring the DIC process.

### *3.2. Results for laminate 1 at various velocities*

The theoretical impact duration was obtained by Wilbeck [20] by assuming that the target is rigid and firmly fixed and that the gelatin flows at its initial velocity during the impact:

$$t_{\text{impact}} = \frac{L_{\text{gel}}}{v_0} \tag{1}$$

where $L_{\text{gel}}$ is the projectile length and $v_0$ the impact velocity.

During the tests, a slightly longer time was measured. To account for the deformation of the plate, the impact duration given by Wilbeck can be modified to account for the additional distance as follows:

$$t_{\text{modified}} = \frac{L_{\text{gel}} + w_{\text{end}}}{v_0} \tag{2}$$

where $w_{\text{end}}$ is the deflection measured at the end of flow calculated by Eq. 1. Estimation of time durations for laminate 1 are given in Tab. 4. Note that experimental evaluation of the impact duration remains rather rough due to the transparency of the gelatin projectile and the visual interpretation of the end of the flow. One must note that both Eq. 1 and Eq. 2 assume that the projectile is impacting the target with its undeformed length $L_{\text{gel}}$ and without any change in velocity, what is questionable as already noticed in

[24]. However, a precise measure of the projectile length at time of impact was not possible with the current set-up. Without surprise, the modification proposed in Eq. 2 to account for the target deformation is greatly improving the evaluation of the impact duration.

| Velocity (m/s) | | Pressure (bar) | Exp. duration (ms) | Eq. 1 (ms) | Diff. w. exp. % | Eq. 2 (ms) | Diff. w. exp. % |
|---|---|---|---|---|---|---|---|
| 87 | | 1.64 | 1.55 | 1.29 | -17% | 1.69 | +9% |
| 92 | | 1.76 | 1.70 | 1.22 | -28% | 1.56 | -8% |
| 96 | | 1.91 | 1.70 | 1.17 | -31% | 1.47 | -14% |
| 99 | (*) | 1.98 | 1.40 | 1.13 | -19% | 1.49 | +6% |
| 106 | (*) | 2.20 | 1.30 | 1.06 | -19% | 1.38 | +6% |
| 112 | (*) | 2.37 | 1.35 | 1.00 | -26% | 1.30 | -4% |

Table 4: Impact duration for laminate 1. (*) indicates tests with large crack noticed.

Fig. 11 shows the time history of center deflection obtained for various impact velocities in the range 87-112 m/s. Dashed lines are used to indicate samples that experienced large failure (at least one large macro-crack of several centimeters) during the impact, as noticed during post-mortem inspections. For the test at 99 m/s, one strain gauge detached from the sample at 1.07 ms due to the shock wave. This did not allow a precise DIC analysis beyond this time. However, shifting the central point by 10 mm from the center to the right gave a very similar curve before 1.07 ms, and allowed the central deflection to be measured beyond detachment of the gauge.

The time to reach maximum deflection is similar for all specimens. The time for returning to zero is also similar, except for 112 m/s. This indicates that, unlike for 112 m/s, the failure mechanisms caused in the case of 99 m/s and 106 m/s did not modify significantly the first natural frequency that

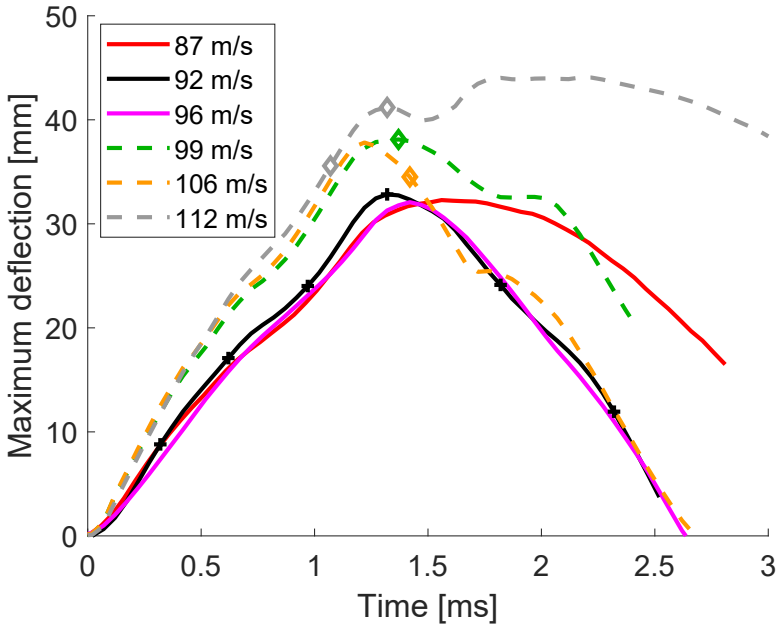


Figure 11: Time history of deflections for laminate 1 impacted at various velocities. Dashed lines show tests in which samples experienced large macro-cracks. "+"-ticks denote time steps of contour plots given in Fig. 9. Diamonds denotes crack visible in fast camera picture.

mainly governs the response of the structure. This is in agreement with the results of quasi-static bending tests by [48] who showed that laminate 1 has a very progressive failure propagation and a very progressive stiffness loss. This is attributed to a good resistance to delamination and, as a consequence, an improved redistribution of stresses in the plies adjacent to a cracked one.

Fig. 12 shows post-mortem photos of the samples that failed. In the case when delamination was noticed, the edges are also shown. Samples impacted below 99 m/s did not fail. At 99 m/s (see the back bace) and 106 m/s (see the impact face) , the samples experienced a major vertical crack -

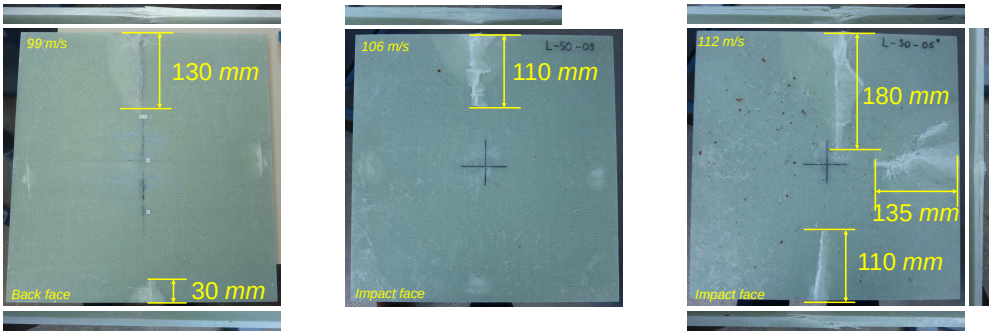


Figure 12: Post-mortem observation of damage on laminate 1 samples: (left) 99 $m/s$, (middle) 106 $m/s$, (right) 112 $m/s$. The side pictures show the edges delamination.

longer than 110 mm - starting from the top middle edge towards the center. In both case, the crack runs through the entire thickness and is visible on the two faces of the sample. Close to the crack, a large white area can be attributed to resin damage. The crack was initiated by the bending of the plate, allowed by the simply supported boundary conditions. The bending resulted in maximum stresses located in the middle of the plate edges (not visible in Fig. 9 as it is hidden by the support plate). Those damages were created by the main bending of the square sample (i.e. mode 1) that led the middle edge zones to experience tension on the back face and compression on the impact face beyond the material yield limit. A second shorter crack is found for 99 m/s. Although it is less energetic than 106 m/s, the larger deflection and larger damage at 99 m/s compared to 106 m/s are attributed to experimental dispersion (projectile excentration, projectile tilted, etc.). [21] showed by SPH simulations that, in the case of gelatin impact on a rigid target, very moderate inclination could change the pressure pulse on the structure although the impact energy and momentum transfer are constant.

At 112 m/s, larger deflections caused three major cracks, all of them starting from the middle of the edges and running through the entire thickness.

Photos of plates' edges show that cracks are accompanied by the presence of delamination mainly located in the mid surface of the plate. It is linked to maximum shear stresses in the mid-plane of the sample and near the edge centres, leading to mode II delamination . As it can be observed in Fig. 12, on the edge, the delamination has almost not propagated beyond the white damage zones, indicating a high interlaminar tenacity.

### *3.3. Laminate 2*

| Velocity (m/s) | | Pressure (bar) | Exp. duration (ms) | Eq. 1 (ms) | Diff. w. exp. % | Eq. 2 (ms) | Diff. w. exp. % |
|---|---|---|---|---|---|---|---|
| 64 | | 0.93 | 2.25 | 1.75 | -22% | 1.98 | -12% |
| 72 | | 1.18 | 1.85 | 1.56 | -16% | 1.81 | -2% |
| 82 | | 1.47 | NA | 1.37 | NA | 1.62 | NA |
| 93 | (*) | 1.83 | 2.50 | 1.21 | -52% | 1.42 | -43% |
| 100 | (*) | 2.02 | 1.90 | 1.12 | -41% | 1.33 | -30% |
| 105 | (*) | 2.19 | 1.35 | 1.07 | -21% | 1.41 | +5% |

Table 5: Impact duration for laminate 2. (*) indicates tests with large crack noticed.

Impact duration measured and calculated for laminate 2 is shown in Tab. 5. As for laminate 1, the theoretical squash up time used by Wilbeck underestimates due to the assumption of rigid target and is improved by modifying the relation according to Eq. 2. However, in the case of failure (see the results for 93, 100, 105 m/s), the improvement given by Eq. 2 is very moderate. As will be shown later with post-mortem observations for laminate 2, failure consisted in major cracks accompanied by large delamination. Also, the time

responses for failed samples show a large drop in the natural frequency of the plate. This indicates a huge change in the global stiffness of the sample that caused large increase in the maximum deflection and, as a consequence, a longer duration.

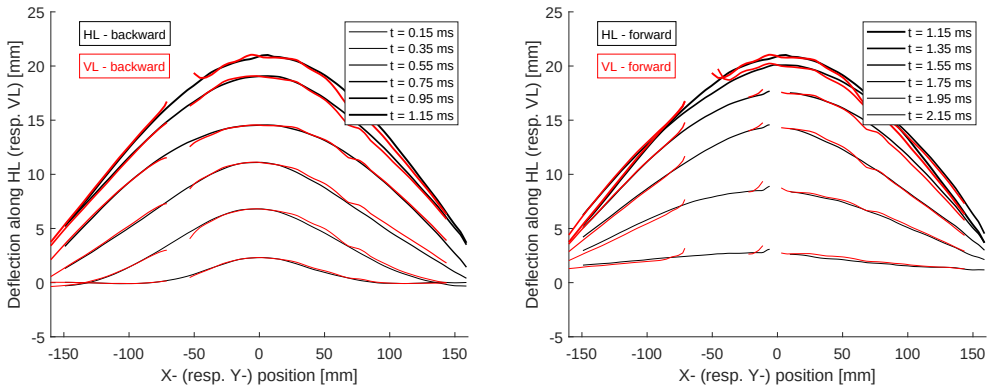


Figure 13: Deflection along horizontal line HL (black) and vertical line VL (red) at various time during the forward (left) and backward (right) motion for laminate 2 impacted at 82 m/s.

Deflection profiles along HL and VL are given in Fig. 13 for the forward (Fig. 13 left) and backward (Fig. 13 right) motion of laminate 2 impacted at 82 m/s. Some parts of the deflection could not be extracted by DIC due to the presence of strain gauges. The horizontal and vertical profiles are clearly similar. This was expected since the stacking in laminate 2 leads to similar stiffnesses in the 0° and 90° directions.

Fig. 14 shows time histories of maximum deflection for laminate 2 impacted in the range 64-105 m/s. For a test at 100 m/s, the fast cameras did not trigged and the DIC extraction is not available. In raw data, the deflection for 93 m/s test increased much slower than for 64, 72 and 82 m/s. The

reason is due to technical issues: the gelatin projectile was very stretched compared to other tests. As a consequence, the impact duration was abnormally longer. However, as shown by [33], it must be noticed that the impact energy and momentum transfer can be considered as independant of the tilt angle and projectile shape. In order to give a correct interpretation of 93 m/s curve, a time scaling was calculated based on the actual length of the projectile approximately measured with front cameras 1 and 2 (see Fig. 4). Impact velocities greater than 93 m/s led to exceeding the yield stress of the samples. Change in slope in Fig. 14 indicates a sudden loss of stiffness due to immediate propagation of cracks and delamination in the sample. This change in slope closely follows the crack initiation noticed in the rear cameras and indicated by diamond ticks in Fig. 14. Consistent with this, the deflections of samples that failed also show a very long time for returning to zero. Theoretically, this response time is mainly linked to the first natural period of composite plates and the duration of the loading. It regularly decreases for unfailed samples when increasing from 64 to 82 m/s as the impact duration decreases. However beyond failure (see for 93 and 105 m/s), the response time largely increases. This is attributed an important drop in the plate stiffness that has two direct consequences. Firstly, the first natural period (that mainly governs the response time) is longer. Secondly, the maximum deflection is largely extended, what increases the impact duration as discussed earlier.

Fig. 15 shows the impact face of the samples observed at 93, 100 and 105 m/s. As for laminate 1, mode 1 bending excited beyond a certain limit led to compressive cracks occuring at the edge centers, running through the

thickness and propagating to the center of the plate. All cracks are accompanied by large delamination, in most cases, along the whole edge. Only large cracks occured even though the velocity range was finely sampled. The first sample failed at 93 m/s along a 190 mm long crack. At 100 and 106 m/s, several cracks are created at the same time, all starting from an edge center. All cracks are accompanied by very large delamination visible from the edges, indicating a low interlaminar strain energy release rate for laminate 2. At this point, two possible scenarios are envisaged. In the first scenario, large deflection of the plate led to excessive bending of the plate edges that initiated folding. Cracks were created in the outer plies due to compressive or tensile stresses and propagated through the thickness as the local stiffness was lost. This also initiated local delamination that immediately propagated. In the second scenario considered, large deflection of the plate led to excessive shear stresses in the corners of the plate, which initiated delamination that immediately propagated. This resulted in a sudden drop of the global stiffness of the plate, that led bending to folding and initiated cracks at the edge centres, propagating towards the plate centre. Eventually, variation of interfacial properties and stress distribution due to the stacking sequence could slightly shift the delamination plane from the exacy geometrical mid-surface of the sample. The dependancy of failure with respect to the impact velocity looks progressive, with a treshold below 93 m/s.

### *3.4. Laminate 3*

Comparisons between experimental impact duration and Eq. 1 and 2 for laminate 3 are given in Tab. 6. As previously, Wilbeck's theory underetimates the impact duration due to the target flexibility. The underestimation

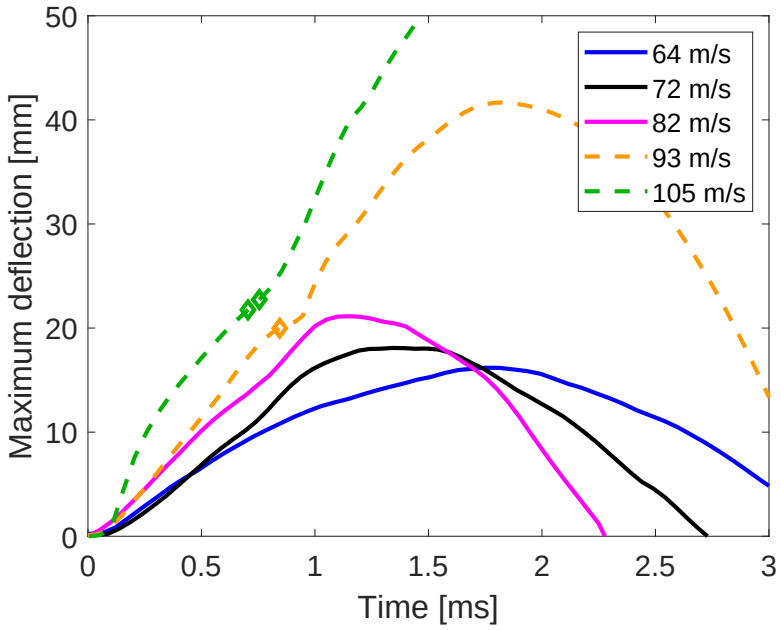


Figure 14: Time history of deflections for laminate 2 impacted at various velocities. Dashed lines show tests in which samples experienced large macro-cracks. Diamonds denotes crack visible in fast camera picture.

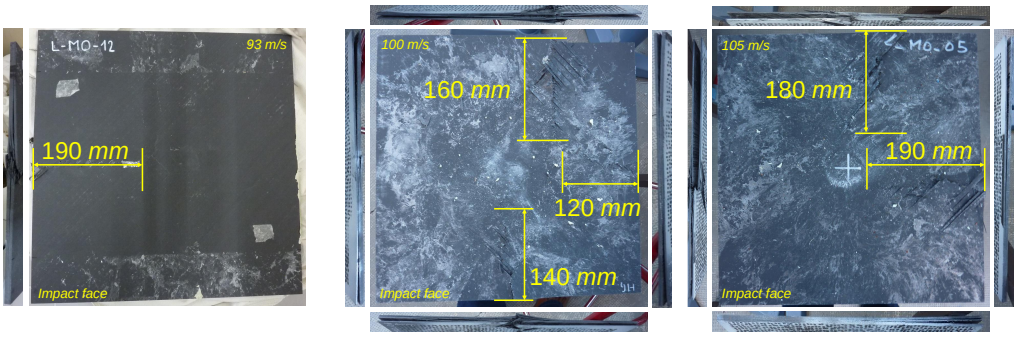


Figure 15: Post-mortem observation of damage on laminate 2 samples: (left) 93 $m/s$, (middle) 100 $m/s$, (right) 105 $m/s$. The side pictures show the edges delamination.

| Velocity (m/s) | | Pressure (bar) | Exp. duration (ms) | Eq. 1 (ms) | Diff. w. exp. % | Eq. 2 (ms) | Diff. w. exp. % |
|---|---|---|---|---|---|---|---|
| 60 | | 0.82 | 2.40 | 1.87 | -22% | 2.09 | -13% |
| 67 | (*) | 1.01 | 1.95 | 1.67 | -14% | 2.19 | +12% |
| 68 | | 1.06 | 2.40 | 1.65 | -31% | 1.91 | -21% |
| 70 | (*) | 1.13 | 2.35 | 1.60 | -32% | 2.14 | -9% |
| 76 | | 1.32 | 1.85 | 1.48 | -20% | 1.75 | -5% |
| 78 | | 1.34 | 1.65 | 1.44 | -13% | 1.71 | +4% |
| 83 | (*) | 1.50 | 2.75 | 1.35 | -51% | 1.77 | -36% |
| 85 | | 1.57 | 1.85 | 1.32 | -29% | 1.58 | -15% |
| 90 | (*) | 1.71 | 2.35 | 1.25 | -47% | 1.62 | -31% |

Table 6: Impact duration for laminate 3. (*) indicates tests with large crack noticed.

is particularly important for samples that failed (i.e. 67, 70, 83 and 90 m/s) because failure led to a loss in stiffness and, as a consequence, an increased deflection. Evaluation by Eq. 2 gives a more precise evaluation of the impact duration, although still underestimating in the case of failure.

Fig. 16 shows the line profile of laminate 3 deflection along VL and HL for the impact at 76 m/s during the forward motion (Fig. 16 left) and backward motion (Fig. 16 right). During the impact, the center of laminate 3 sample deflects first. However, the stiffness is different in 0° and 90° direction due to preferential 0° fibre reinforcement, with 0° corresponding to the vertical direction. As a consequence, the deflection is clearly more distributed along the 0° direction (i.e. VL direction), in particular in the forward part of the impact.

Fig. 17 shows the time history of deflections for laminate 3 for gelatin impacts in the range 60-90 m/s. Maximum deflection takes place at approx-

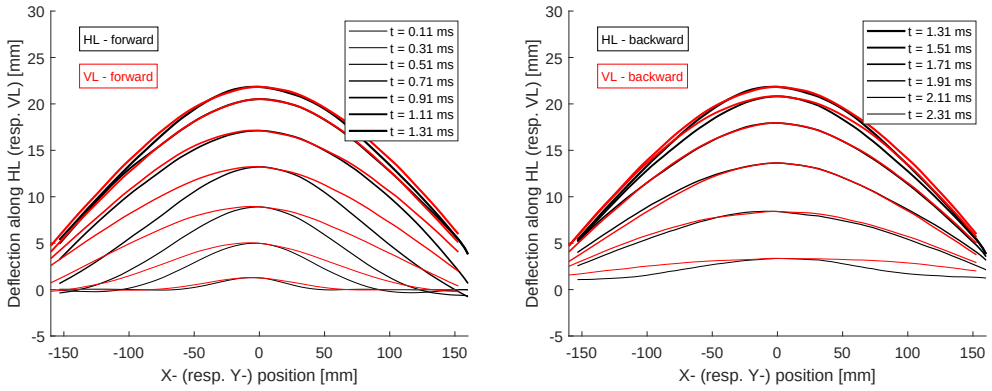


Figure 16: Deflection along horizontal line HL (black) and vertical line VL (red) at various time during the forward (left) and backward (right) motion for laminate 3 impacted at 76 m/s.

imately 1300 $\mu$s. After that, the plate deforms backwards to zero except in the case of large cracks causing the loss of stiffness and, as a consequence, of strain energy. Dashed lines show tests in which samples experienced large macro-cracks or extended delamination. As expected, at the beginning, the deflection slope increases with the impact velocity. However, contrary to laminates 1 and 2, failure occured in random order: the sample impacted at 67 m/s failed, but the one at 85 m/s sustained without any visible damage. This "non-deterministic" failure behavior is attributed to a "all or none" behavior of laminate 3 UD material: as soon as damage or delamination initiates, it immediatly propagates and leads to the complete failure of the sample. In particular, dispersion in the interlaminar properties of the material would lead to impredictable sudden stiffness drop of the samples. This behavior was also noticed during quasi-static bending tests performed on beam samples of the same material [48]. In addition, random imperfections

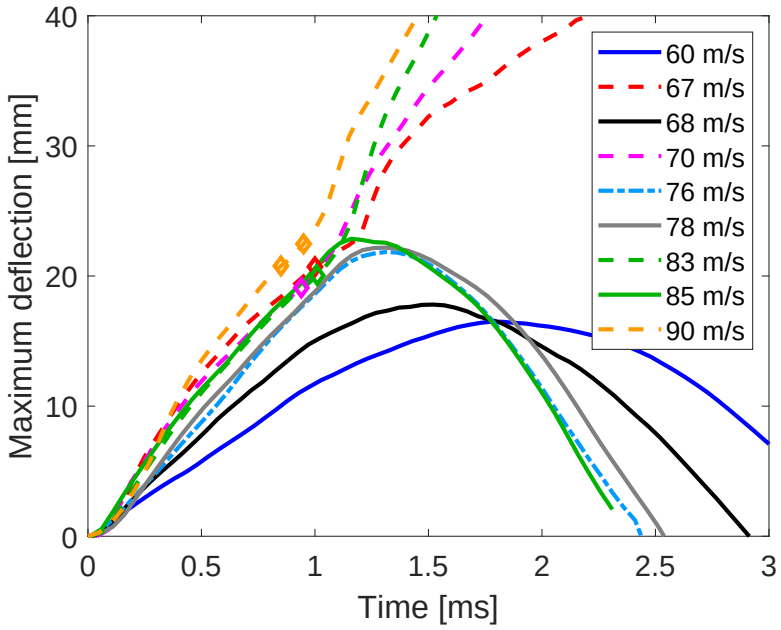


Figure 17: Time history of deflections for laminate 3 impacted at various velocities. Dashed lines show tests in which samples experienced large macro-cracks. The dash-dotted curve (76 m/s) corresponds to a sample experienced only delamination. Diamonds denotes times when crack seemed to appear on the camera picture.

(in particular porosities) in the material and experimental dispersion (projectile tilt for instance) are expected to increase this chaotic behavior. This immediate propagation to quasi-complete failure is directly responsible for the change in slope points in time histories (see Fig. 17) for 67, 70, 83, 90 m/s tests around 20-25 mm deflection. As for laminate 2, the response time slightly decreases for unfailed samples. In this case, the samples should have the same natural period, but the duration of the loading – related to the impact duration - slightly increases. However for failed samples, the response

485 time largely increases, and eventually the deflection did not come back to
486 zero when the loss in stiffness was too large.

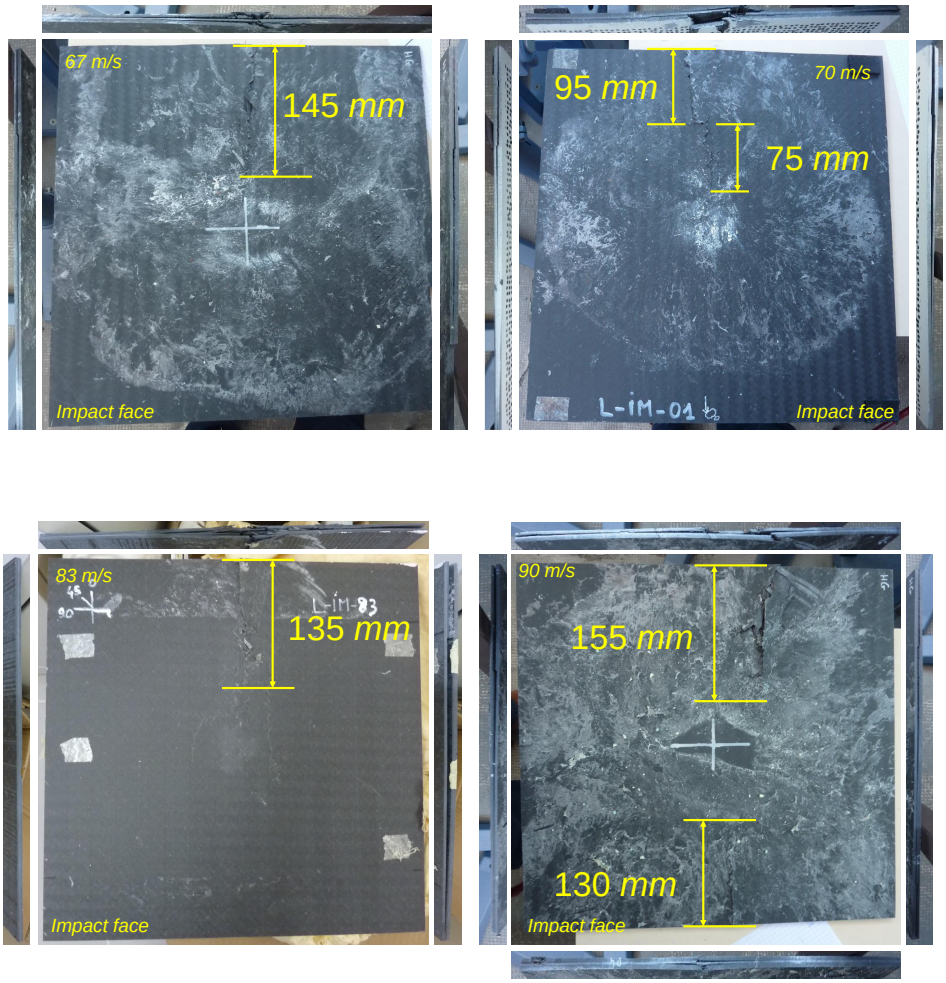


Figure 18: Post-mortem observation of damage on laminate 3 samples: (upper left) 67 $m/s$, bottom left 70 $m/s$, (upper right) 83 $m/s$, (bottom right) 90 $m/s$. The side pictures show the edges delamination.

487 Fig. 18 shows the impact faces and delaminated edges during post-

mortem inspection of the plates that failed. Despite the very moderate increase in the impact velocity, only long cracks occured, always longer than 130 mm. For 70 m/s, the first 95 mm crack "recentered" in a horizontal bifurcation and then continued vertically towards the center of the plate. At 90 m/s, two vertical cracks were created at the top and bottom edges. It should be noticed that only vertical cracks occured. As noticed on the deformed shape, laminate 3 stiffness is different in 0° and 90° directions. This difference has directly driven the directions of the cracks appearance as being caused by bending in the weakest direction (90°), what led to long cracks along the 0° direction. From the edges' pictures, all cracks were accompanied by large delamination between the mid plies of the samples, with possibly some bifurcation here and there.

Note that for the impact at 76 m/s, large delamination was noticed along the edges without any crack in the facesheets. However, no difference with undamaged plates can be noticed in the time history (Fig. 11), indicating that the stiffness was globally maintained. This tends to indicate that in laminate 3, delamination occured first, then followed by cracks initiation and immediate propagation, what led to a sudden drop in the stiffness.

For laminate 3, delamination was never located in the exact mid-surface interface which is between two plies in 0° direction. In all cases, even when initiated by the large cracks, the delaminated interface was between a 0° ply and a 90° ply, or between a unidirectional ply (at 0°) and a fabric ply (at $\pm 45°$).

## 4. Conclusion

This paper provides a detailed analysis of 21 gelatin impact tests performed on three laminated composite configurations at several velocities up to complete failure. One objective of this paper is to open the experimental data to the readers for comparison with other tests or numerical models. The experimental data from DIC analysis are available on the *Recherche Data Gouv* website at the following URL [43]: https://doi.org/10.57745/UA1CRZ.

Some conclusions can be drawn:

- for transient dynamic experiments, DIC analysis provides a very detailed experimental information. The field data extracted is able to capture both the time and space variations, what should be considered of key interest for the validation of numerical models.

- DIC analysis was shown to finely capture the strain field on the back face of the sample; as a consequence, strain gauges could be removed.

- neglecting the target flexibility leads to high underestimation of the impact duration by around -20% to -30% or more with Wilbeck's relation. Based on the deflection recorded during the test, a modified equation was proposed that improves the estimation of impact duration.

- failure mechanisms were different for the materials tested: for glass/epoxy plain weave fabrics laminate, bending led to cracking the outer plies by global folding of the plate, without extended delamination. For the carbon/epoxy materials, delamination seemed to occur first and to propagate immediately, then leading to large bending and loss of stiffness. A fine prediction of such failure mechanisms based on material

models is a challenge. In particular for laminate 3, failure occured in a non progressive way with respect to impact speed. Such dispersion can not be solely attributed to experimental hazards. Dispersion in the materials properties are currently being investigated to explain the failure noticed.

Continuation of this study is currently under progress, with other materials tested, and an improvement of the experimental set-up with force sensors. A multiscale numerical model involving the failure mechanisms is also undertaken.

## CRediT authorship contribution statement

**O. Dorival** Conceptualization, Methodology, State of the art, experiments preparation, experimental campaign, post-treatment, validation, funding acquisition, project management, writing - original draft, writing - review & editing. **P. Navarro** Experiments preparation, experimental campaign, writing - review & editing. **S. Marguet** Set-up design, experimental campaign, post-treatment, writing - review & editing. **J.-F. Ferrero** Conceptualization, Methodology, Experimental campaign, funding acquisition, supervision, writing - review & editing.

## Acknowledgements

This research work has been conducted with the financial grant of DGA Naval Systems, France, within the framework of the DGA RAPID project named SUCCESS. The authors would also like to express their gratitude

to the engineering design office Meca (www.calcul-meca.fr) and Multiplast company for their technical assistance.

## Declaration of Competing Interest

The authors declare that they have no known competing financial interests or personal relationships that could have appeared to influence the work reported in this paper.

## References

[1] P. Wang, C. Lian, C. Yue, X. Wu, J. Zhang, K. Zhang, Z. Yue, Experimental and numerical study of tire debris impact on fuel tank cover based on coupled eulerian-lagrangian method, International Journal of Impact Engineering 157 (2021) 103968. URL: https://www.sciencedirect.com/science/article/pii/S0734743X2100155X. doi:https://doi.org/10.1016/j.ijimpeng.2021.103968.

[2] L. Wu, D. Huang, F. Bobaru, A reformulated rate-dependent visco-elastic model for dynamic deformation and fracture of pmma with peridynamics, International Journal of Impact Engineering 149 (2021) 103791. URL: https://www.sciencedirect.com/science/article/pii/S0734743X20308617. doi:https://doi.org/10.1016/j.ijimpeng.2020.103791.

[3] I. Mohagheghian, Y. Wang, J. Zhou, L. Yu, X. Guo, Y. Yan, M. Charalambides, J. Dear, Deformation and damage mechanisms of laminated glass windows subjected to high velocity

soft impact, International Journal of Solids and Structures 109 (2017) 46–62. URL: https://www.sciencedirect.com/science/article/pii/S0020768317300082. doi:https://doi.org/10.1016/j.ijsolstr.2017.01.006.

[4] I. Mohagheghian, M. Charalambides, Y. Wang, L. Jiang, X. Zhang, Y. Yan, A. Kinloch, J. Dear, Effect of the polymer interlayer on the high-velocity soft impact response of laminated glass plates, International Journal of Impact Engineering 120 (2018) 150–170. URL: https://www.sciencedirect.com/science/article/pii/S0734743X18300265. doi:https://doi.org/10.1016/j.ijimpeng.2018.06.002.

[5] N. Ahmed, P. Xue, Determination of the size of the local region for efficient global/local modeling in a large composite structure under impact loading, International Journal of Impact Engineering 144 (2020) 103646. URL: https://www.sciencedirect.com/science/article/pii/S0734743X18312181. doi:https://doi.org/10.1016/j.ijimpeng.2020.103646.

[6] J. LIU, Y. LI, X. YU, X. GAO, Z. LIU, Design of aircraft structures against threat of bird strikes, Chinese Journal of Aeronautics 31 (2018) 1535–1558. URL: https://www.sciencedirect.com/science/article/pii/S1000936118301614. doi:https://doi.org/10.1016/j.cja.2018.05.004.

[7] X. Meng, Y. Sun, J. Yu, Z. Tang, J. Liu, T. Suo, Y. Li, Dynamic response of the horizontal stabilizer during uas air-

borne collision, International Journal of Impact Engineering 126 (2019) 50–61. URL: https://www.sciencedirect.com/science/article/pii/S0734743X18305098. doi:https://doi.org/10.1016/j.ijimpeng.2018.11.015.

[8] M. S. Tatlier, T. Baran, Structural and cfd analysis of an airfoil subjected to bird strike, European Journal of Mechanics - B/Fluids 84 (2020) 478–486. URL: https://www.sciencedirect.com/science/article/pii/S0997754619307721. doi:https://doi.org/10.1016/j.euromechflu.2020.07.012.

[9] R. Vignjevic, M. Or?owski, T. De Vuyst, J. C. Campbell, A parametric study of bird strike on engine blades, International Journal of Impact Engineering 60 (2013) 44–57. URL: https://www.sciencedirect.com/science/article/pii/S0734743X13000870. doi:https://doi.org/10.1016/j.ijimpeng.2013.04.003.

[10] L. Liu, G. Luo, W. Chen, Z. Zhao, X. Huang, Dynamic behavior and damage mechanism of 3d braided composite fan blade under bird impact, International Journal of Aerospace Engineering 2018 (2018) 5906078–. URL: https://doi.org/10.1155/2018/5906078. doi:10.1155/2018/5906078.

[11] P. Davies, Composites for Marine Applications, Springer Netherlands, Dordrecht, 1999, pp. 235–248. URL: https://doi.org/10.1007/978-94-011-4489-6_12. doi:10.1007/978-94-011-4489-6_12.

[12] G. Gupta, A. Kumar, R. Tyagi, S. Kumar, Application and future

of composite materials: A review, International Journal of Innovative Research in Science, Engineering and Technology 5 (2016) 6907–6911.

[13] R. Masilamani, N. Dhandapani, K. V. Kumar, K. T. Mani, A review on usage of carbon fiber reinforced plastics in automobiles, International Journal of Pure and Applied Mathematics 117 (2017) 537–544.

[14] M. Fuwa, A. Bunsell, B. Harris, Tensile failure mechanisms in carbon fibre reinforced plastics, J. Mater. Sci. 10 (1975) 2062–2070. doi:https://doi.org/10.1007/BF00557484.

[15] D. Gay, Composite Materials: Design and Applications (4th ed.)., CRC Press, Boca Raton, 2022. doi:https://doi.org/10.1201/9781003195788.

[16] S. Abrate, Soft impacts on aerospace structures, Progress in Aerospace Sciences 81 (2016) 1–17. URL: https://www.sciencedirect.com/science/article/pii/S0376042115300294. doi:https://doi.org/10.1016/j.paerosci.2015.11.005, dynamic Loading Aspects of Composite Materials.

[17] I. C. Metz, J. Ellerbroek, T. Mühlhausen, D. Kügler, J. M. Hoekstra, The bird strike challenge, Aerospace 7 (2020). URL: https://www.mdpi.com/2226-4310/7/3/26. doi:10.3390/aerospace7030026.

[18] J. P. Barber, H. R. Taylor, J. S. Wilbeck, Characterization of bird impacts on a rigid plate: Part 1, in: Technical report AFFDL-TR-75-5, Air Force Flight Dynamics Laboratory, Wright-Patterson Air Force Base, OH, 1975.

[19] R. L. Peterson, J. P. Barber, Bird impact forces in aircraft windshield design, in: Technical report AFFDL-TR-75-150, Air Force Flight Dynamics Laboratory, Wright-Patterson Air Force Base, OH, 1976.

[20] J. S. Wilbeck, Impact behavior of low strength projectiles., in: Technical report AFML-TR-77-134, Air Force Materials Laboratory, Wright-Patterson Air Force Base, OH, 1978.

[21] F. Allaeys, G. Luyckx, W. Van Paepegem, J. Degrieck, Numerical and experimental investigation of the shock and steady state pressures in the bird material during bird strike, International Journal of Impact Engineering 107 (2017) 12–22. URL: https://www.sciencedirect.com/science/article/pii/S0734743X16308843. doi:https://doi.org/10.1016/j.ijimpeng.2017.05.006.

[22] S. Heimbs, Computational methods for bird strike simulations: A review, Computers & Structures 89 (2011) 2093–2112. doi:https://doi.org/10.1016/j.compstruc.2011.08.007.

[23] C. J. Welsh, V. Centonze, Aircraft transparency testing - artificial birds. report aedc-tr-86-2, us air force, in: Technical report AEDC-TR-86-2, Arnold Engineering Development Center, Arnold Air Force Station, TN, 1986.

[24] M. Lavoie, A. Gakwaya, M. N. Ensan, D. Zimcik, D. Nandlall, Bird's substitute tests results and evaluation of available numerical methods, International Journal of Impact Engineering 36 (2009) 1276–1287. URL: https://www.sciencedirect.com/science/

673 article/pii/S0734743X0900058X. doi:https://doi.org/10.1016/j.
674 ijimpeng.2009.03.009.

675 [25] G. D. Roberts, J. M. Pereira, D. M. Revilock, W. K. Binienda, M. Xie,
676 M. Braley, Ballistic impact of braided composites with a soft projectile,
677 Journal of Aerospace Engineering 18 (2005) 3–7. doi:10.1061/(ASCE)
678 0893-1321(2005)18:1(3).

679 [26] S. Zhu, M. Tong, Y. Wang, Experiment and Numerical Simula-
680 tion of a Full-Scale Aircraft Windshield Subjected to Bird Impact,
681 ???? URL: https://arc.aiaa.org/doi/abs/10.2514/6.2009-2575.
682 doi:10.2514/6.2009-2575.

683 [27] D. Hu, B. Song, D. Wang, Z. Chen, Experiment and numeri-
684 cal simulation of a full-scale helicopter composite cockpit structure
685 subject to a bird strike, Composite Structures 149 (2016) 385–
686 397. URL: https://www.sciencedirect.com/science/article/pii/
687 S0263822316303269. doi:https://doi.org/10.1016/j.compstruct.
688 2016.04.035.

689 [28] J. Liu, Y. Li, X. Yu, Z. Tang, X. Gao, J. Lv, Z. Zhang, A
690 novel design for reinforcing the aircraft tail leading edge structure
691 against bird strike, International Journal of Impact Engineering
692 105 (2017) 89–101. URL: https://www.sciencedirect.com/science/
693 article/pii/S0734743X16310995. doi:https://doi.org/10.1016/j.
694 ijimpeng.2016.12.017, design and Analysis of Protective Structures
695 2015.

[29] Y. Liu, J. Qu, X. Yan, Y. Pang, P. Yang, Study on dynamic response characteristics of bird impact glass fiber laminate, Journal of Physics: Conference Series 1676 (2020) 012178. URL: https://dx.doi.org/10.1088/1742-6596/1676/1/012178. doi:10.1088/1742-6596/1676/1/012178.

[30] E. Giannaros, A. Kotzakolios, V. Kostopoulos, G. Sotiriadis, R. Vignjevic, N. Djordjevic, M. Boccaccio, M. Meo, Low- and high-fidelity modeling of sandwich-structured composite response to bird strike, as tools for a digital-twin-assisted damage diagnosis, International Journal of Impact Engineering 160 (2022) 104058. URL: https://www.sciencedirect.com/science/article/pii/S0734743X21002451. doi:https://doi.org/10.1016/j.ijimpeng.2021.104058.

[31] R. Vignjevic, J. Campbell, K. Hughes, M. Or?owski, S. Garcea, P. Withers, J. Reed, Soft body impact resistance of composite foam core sandwich panels with unidirectional corrugated and tubular reinforcements, International Journal of Impact Engineering 132 (2019) 103320. URL: https://www.sciencedirect.com/science/article/pii/S0734743X19301800. doi:https://doi.org/10.1016/j.ijimpeng.2019.103320.

[32] M. Anghileri, G. Sala, Theoretical assessment, numerical simulation and comparison with tests of birdstrike on deformable structures, in: Proceedings of the 20th Congress of the International Council of the Aeronautical Sciences (ICAS 96), 1996.

[33] F. Allaeys, G. Luyckx, W. Van Paepegem, J. Degrieck, Characterization of real and substitute birds through experimental and numerical analysis of momentum, average impact force and residual energy in bird strike on three rigid targets: A flat plate, a wedge and a splitter, International Journal of Impact Engineering 99 (2017) 1–13. URL: https://www.sciencedirect.com/science/article/pii/S0734743X16303165. doi:https://doi.org/10.1016/j.ijimpeng.2016.08.009.

[34] D. Nandlall, A. Gakwaya, On the determination of the shock and steady state parameters of gelatine from cylinder impact experiments, International Journal of Impact Engineering 116 (2018) 22–33. URL: https://www.sciencedirect.com/science/article/pii/S0734743X17309028. doi:https://doi.org/10.1016/j.ijimpeng.2018.02.001.

[35] J. Pernas-Sanchez, J. Artero-Guerrero, D. Varas, J. Lopez-Puente, Artificial bird strike on hopkinson tube device: Experimental and numerical analysis, International Journal of Impact Engineering 138 (2020) 103477. URL: https://www.sciencedirect.com/science/article/pii/S0734743X19308280. doi:https://doi.org/10.1016/j.ijimpeng.2019.103477.

[36] J. Field, S. Walley, W. Proud, H. Goldrein, C. Siviour, Review of experimental techniques for high rate deformation and shock studies, International Journal of Impact Engineering 30 (2004) 725–775. URL: https://www.sciencedirect.com/science/

744 article/pii/S0734743X04000521. doi:https://doi.org/10.1016/j.
745 ijimpeng.2004.03.005, fifth International Symposium on Impact En-
746 gineering.

747 [37] F. Hild, A. Bouterf, S. Roux, Measurement of kinematic fields
748 via dic for impact engineering applications, International Journal
749 of Impact Engineering 130 (2019) 163–171. URL: https://www.
750 sciencedirect.com/science/article/pii/S0734743X1831087X.
751 doi:https://doi.org/10.1016/j.ijimpeng.2019.04.007.

752 [38] H. Xin, J. Tao, M. Xiaomin, S. Xuefeng, L. Xin, Dynamic re-
753 sponse of single curved fiber-metal hybrid lamina composites subject
754 to low-velocity impact, International Journal of Impact Engineering
755 164 (2022) 104209. URL: https://www.sciencedirect.com/science/
756 article/pii/S0734743X22000550. doi:https://doi.org/10.1016/j.
757 ijimpeng.2022.104209.

758 [39] H. Arora, P. A. Hooper, J. P. Dear, The effects of air and un-
759 derwater blast on composite sandwich panels and tubular laminate
760 structures, Experimental Mechanics 52 (2012) 59–81. URL: https:
761 //doi.org/10.1007/s11340-011-9506-z. doi:https://doi.org/10.
762 1007/s11340-011-9506-z, dynamic Loading Aspects of Composite Ma-
763 terials.

764 [40] M. Louar, B. Belkassem, H. Ousji, K. Spranghers, D. Kakogiannis,
765 L. Pyl, J. Vantomme, Explosive driven shock tube loading of aluminium
766 plates: experimental study, International Journal of Impact Engineering
767 86 (2015) 111–123. URL: https://www.sciencedirect.com/science/

768 article/pii/S0734743X15001682. doi:https://doi.org/10.1016/j.
769 ijimpeng.2015.07.013.

770 [41] D. Delsart, F. Boyer, A. Vagnot, Assessment of a suibstitute bird model
771 for the prediction of bird-strike of helicopters structures, in: Proceed-
772 ings of the 7th International Conference on Mechanics and Materials in
773 Design. Albufeira/Portugal 11-15 June 2017, 2017.

774 [42] J. Zhou, J. Liu, X. Zhang, Y. Yan, L. Jiang, I. Mohagheghian,
775 J. Dear, M. Charalambides, Experimental and numerical in-
776 vestigation of high velocity soft impact loading on aircraft ma-
777 terials, Aerospace Science and Technology 90 (2019) 44–
778 58. URL: https://www.sciencedirect.com/science/article/pii/
779 S1270963818327147. doi:https://doi.org/10.1016/j.ast.2019.04.
780 015.

781 [43] O. Dorival, P. Navarro, S. Marguet, J.-F. Ferrero, 3D digital image
782 correlation of soft impact test on composite plates, 2023. URL: https:
783 //doi.org/10.57745/UA1CRZ. doi:10.57745/UA1CRZ.

784 [44] L. Marquez Duque, H. Le Sourne, J.-C. Petiteau, Arbitrary lagrangian
785 eulerian method to study gel projectile impacts against composite naval
786 plates, in: Proceedings of the 7th ECCOMAS Thematic Conference on
787 the Mechanical Response of Composites. Girona, Spain., 2019.

788 [45] A. M. Amaro, P. N. B. Reis, A. G. Magalhães, M. F. S. F. de Moura, The
789 influence of the boundary conditions on low-velocity impact composite
790 damage, Strain 47 (2011) e220–e226. URL: https://onlinelibrary.

wiley.com/doi/abs/10.1111/j.1475-1305.2008.00534.x.
doi:https://doi.org/10.1111/j.1475-1305.2008.00534.x.
arXiv:https://onlinelibrary.wiley.com/doi/pdf/10.1111/j.1475-1305.2008.00534.x

[46] T. M. Pham, H. Hao, Effect of the plastic hinge and boundary conditions on the impact behavior of reinforced concrete beams, International Journal of Impact Engineering 102 (2017) 74–85. URL: https://www.sciencedirect.com/science/article/pii/S0734743X16305851. doi:https://doi.org/10.1016/j.ijimpeng.2016.12.005.

[47] K. R. Kaware, M. S. Kotambkar, Effect of impactor velocity and boundary condition on low velocity impact finite element modelling of cfrp composite laminates, IOP Conference Series: Materials Science and Engineering 1004 (2020) 012018. URL: https://dx.doi.org/10.1088/1757-899X/1004/1/012018. doi:10.1088/1757-899X/1004/1/012018.

[48] G. Barlow, O. Dorival, G. Kemlin, Endommagements de composites stratifiés et sandwiches sous impacts de gélatine moyenne vitesse, in: 21ème Journées Nationales sur les Composites, École Nationale Supérieure d'Arts et Métiers (ENSAM) - Bordeaux, Bordeaux, Talence, France, 2019. URL: https://hal.science/hal-02420804.